

---

# Environmental effects on emergent strategy in micro-scale multi-agent reinforcement learning

---

**Samuel Tovey**

Institute for Computational Physics  
University of Stuttgart  
Stuttgart, Germany 70569  
stovey@icp.uni-stuttgart.de

**David Zimmer**

Institute for Computational Physics  
University of Stuttgart  
Stuttgart, Germany 70569  
dzimmer@icp.uni-stuttgart.de

**Christoph Lohrmann**

Institute for Computational Physics  
University of Stuttgart  
Stuttgart, Germany 70569  
clorhmann@icp.uni-stuttgart.de

**Tobias Merkt**

Institute for Computational Physics  
University of Stuttgart  
Stuttgart, Germany 70569  
tmerkt@icp.uni-stuttgart.de

**Simon Koppenhöfer**

Institute for Computational Physics  
University of Stuttgart  
Stuttgart, Germany 70569  
skoppenheofer@icp.uni-stuttgart.de

**Veit-Lorenz Heuthe**

Department of Physics - Soft Condensed Matter  
Universität Konstanz  
Konstanz, Germany

**Clemens Bechinger**

Department of Physics - Soft Condensed Matter  
Universität Konstanz  
Konstanz, Germany

**Christian Holm**

Institute for Computational Physics  
University of Stuttgart  
Stuttgart, Germany 70569  
holm@icp.uni-stuttgart.de

## Abstract

Multi-Agent Reinforcement Learning (MARL) is a promising candidate for realizing efficient control of microscopic particles, of which micro-robots are a subset. However, the microscopic particles' environment presents unique challenges, such as Brownian motion at sufficiently small length-scales. In this work, we explore the role of temperature in the emergence and efficacy of strategies in MARL systems using particle-based Langevin molecular dynamics simulations as a realistic representation of micro-scale environments. To this end, we perform experiments on two different multi-agent tasks in microscopic environments at different temperatures, detecting the source of a concentration gradient and rotation of a rod. We find that at higher temperatures, the RL agents identify new strategies for achieving these tasks, highlighting the importance of understanding this regime and providing insight into optimal training strategies for bridging the generalization gap between simulation and reality. We also introduce a novel Python package for studying microscopic agents using reinforcement learning (RL) to accompany our results.

## 1 Introduction

In recent years, machine learning (ML) and physics have enjoyed a strong relationship in broad fields ranging from quantum chemistry [Zaverkin et al., 2023] to cosmology [Krippendorf and Spannowsky, 2022]. An emerging application of ML in the physical sciences is understanding the dynamics and collective behavior of microscopic particles or colloids [Zöttl and Stark, 2023]. In these low Reynolds number regimes, the physics of Brownian motion and hydrodynamics dominate, leading to exciting challenges [Brewer et al., 2022]. Despite these challenges, unusual collective behavior has been observed in both biological [Sugi et al., 2021] and artificial [Zöttl and Stark, 2016] active matter environments. A current research area in this field is understanding how to program these artificial microscopic colloids or agents to achieve tasks like locating positions in an environment or moving objects. Such detailed control over microscopic agents can revolutionize many fields, with medicine being of great interest [Soto et al., 2020]. While there has been a significant amount of progress utilizing classical algorithms [Moreau et al., 2021, Lolli et al., 2022], recently, reinforcement learning (RL) has become a promising candidate [Qin et al., 2023, Hartl et al., 2021, Borra et al., 2022, Muiños-Landin et al., 2021]. Most RL approaches thus far have centered around using Q-learning for single-agent tasks. However, effective deployment of these agents will likely involve collective behavior and, therefore, a multi-agent setting. Furthermore, the role of the environment in these tasks has yet to be investigated to a great extent, partially due to many groups relying on experimental implementations of these agents and, therefore, not having access to such variables. This also prohibits the training time of the models, as experimentally driven RL is laborious. In this work, we approach the problem of understanding how the Brownian motion of these agents impacts their emergent strategy and its efficacy at different temperatures. We utilize a powerful physics engine designed to study these systems, ESPResSo [Weik et al., 2019], to perform these experiments at scale. Experiments involve implementing MARL for the problems of detecting target points in a box and rotating a rod.

Our main contributions are:

- We demonstrate emergent collective behavior in RL-driven micro-robots in realistic simulations.
- We discuss the role of Brownian motion in the agents’ success in their tasks.
- We demonstrate the robustness of MARL algorithms against environmental noise.
- We highlight the differences in emergent strategies as a function of temperature and comment on this as a necessary consideration in bridging the generalization gap with experiments.

All of the infrastructure for the work performed in this investigation is packaged into an open-source Python project, SwarmRL, which is available publicly on GitHub.

## 2 Related Work

Much work has been dedicated to both emergent strategy in microscopic agents and the application of RL at these length scales. A lot of this work has focused on understanding relationships between artificial microswimmers and their biological counterparts or applying simplified RL strategies such as Q-learning to various problems.

**Collective Behaviour in Artificial Microswimmers** Understanding the behavior of organisms on microscopic scales has been a central research focus since the early 1900s. In recent years, with the invention of artificial microswimmers, improved imaging methods, and advanced computational systems, one has been able to probe these behaviors in much greater detail. Of particular interest is the emergence of collective behavior in groups of microswimmers; that is, with limited local information about their environments, groups of agents can share knowledge to achieve a task. In Lavergne et al. [2019] and Bäuerle et al. [2020], group formation and behavior were studied utilizing classical interaction algorithms for microswimmers under varying conditions. These studies demonstrated the emergence of collective behavior for swimmers with varying degrees of sensory ability. In their 2022 paper, Chen and Bechinger [2022] investigated the response of microscopic swarms to external threats. This work emphasized that collective groups of microswimmers use information sharing to respond to events that individuals may not be aware of. In each of these studies, while the effects

of Brownian motion are implicit in the setup, the role of these fluctuations is not explored, nor is a specific task programmed.

**Microscopic RL** In the direction of RL, several studies have approached the problem of organizing microswimmers to the end of achieving a goal. These studies typically rely on RL as a policy development algorithm. Qin et al. [2023] utilize a Q-learning algorithm to learn the swimming strategies of microswimmers and identify new swimming gaits for linked artificial micro-robots. In the direction of learning policy, Hartl et al. [2021] have used a genetic algorithm to reproduce biological chemo-taxis in artificial swimmers and Borra et al. [2022] implement actor-critic RL on a predator-prey problem and found that agents could utilize hydrodynamic cues to avoid predators in their environment. Finally, Muiños-Landin et al. [2021] utilized a Q-learning approach to study how the environments of microswimmers impact their learning process for individual swimmer tasks, including the role of Brownian motion. However, they did not investigate the impact on collective behavior or for more complex tasks which require algorithms beyond Q-learning.

To date, the role of the stochastic forces experienced by microswimmers in their emergent strategy has yet to be investigated. However, these forces are a crucial component of micro-robotics, and therefore, their impact on learning is identified here as the primary research gap we aim to fill.

### 3 Problem Description

Controlling multi-agent systems is a challenging task in-and-of itself. Additionally, on microscopic agents' length scales, thermal fluctuations are relevant. To varying degrees they will prohibit agents from performing a task by introducing a random component preventing the outcome of an action from being predicted with certainty. On the contrary, the existence of this Brownian motion will encourage exploration of the agents as each action they take is perturbed.

We study numerically a system comprising colloids on the micrometer scale that can perform actions such as actively moving or rotating. Using RL, we want to enable the colloids to solve tasks like finding the source of an attractant or rotating a rod. We set out to understand the role of thermal fluctuations in the efficacy of RL on microscopic scales and the emergent strategy adopted by the agents.

In all simulations, a Langevin thermostat correctly reproduces the agents' Brownian motion and maintains the system's temperature in a statistical physics sense. More broadly, stochastic effects can also occur at length scales where thermal motion is not relevant, for example imperfect motors or sensors on a robot. Our work is therefore also relevant for applications beyond the micro-scale.

## 4 Methods

The successful implementation of these experiments has required many unique components. Here we outline briefly the critical aspects of the work.

### 4.1 Particle Simulations

We simulate the trajectories of particles using the overdamped Langevin equations of motion for position and orientation

$$\dot{\mathbf{r}}_i = \frac{1}{\gamma_t} [F(t)\mathbf{e}_i(\Theta_i) - \nabla V(\mathbf{r}_i, \{\mathbf{r}_j\})] + \sqrt{2k_B T / \gamma_t} \mathbf{R}_i^t(t), \quad (1)$$

$$\dot{\Theta} = \frac{1}{\gamma_r} \tau(t) + \sqrt{2k_B T / \gamma_r} R_i^r(t). \quad (2)$$

Here,  $\mathbf{r}_i$  is the (two-dimensional) position of particle  $i$ ,  $\Theta_i$  the angle describing the particle orientation,  $\gamma_{(t,r)}$  the translational (rotational) friction coefficient,  $F$  and  $\tau$  an active force and torque corresponding to an action,  $\mathbf{e} = (\cos(\Theta), \sin(\Theta))^T$  the particle orientation,  $V$  an interaction potential between all particles in the system,  $k_B$  the Boltzmann constant,  $T$  the temperature and  $\mathbf{R}_i^{(t,r)}$  a noise term with zero mean and correlations according to  $\langle R_i^{(t,r)}(t) R_j^{(t,r)}(t') \rangle = \delta_{ij} \delta(t - t')$ , where  $\langle \cdot \rangle$

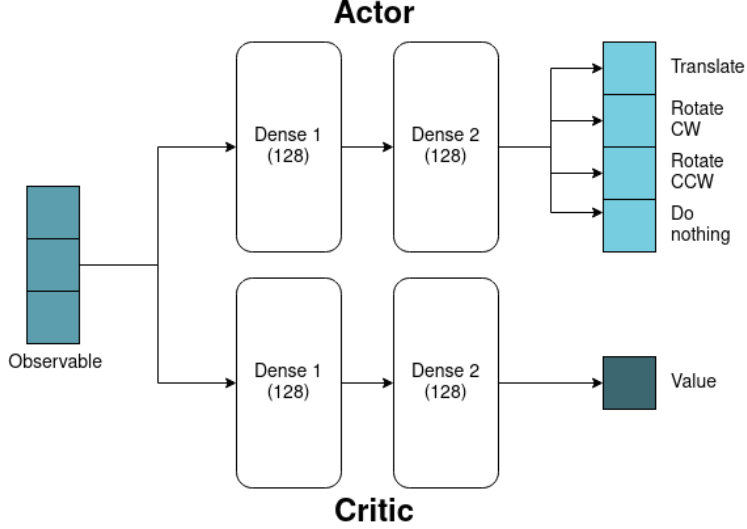


Figure 1: The workflow of the MARL utilized in the experiments. An observable is passed to an actor and a critic, each composed of two dense layers with 128 units. The actor returns a probability of selecting each of the four actions and the critic returns the estimated value of the state.

denotes an ensemble average. For colloids of radius  $a$  in a fluid with dynamic viscosity  $\mu$  we calculate the friction coefficient according to Stokes' law as  $\gamma_t = 6\pi\mu a$  and  $\gamma_r = 8\pi\mu a^3$ .

Equations (1) and (2) are solved numerically using the ESPResSo [Weik et al., 2019] simulation package with a time-step  $\delta t = 0.01$  s, the actions that determine  $F(t)$  and  $\tau(t)$  are updated every time slice  $\Delta t = 1$  s. In all cases, unless otherwise specified, when referring to time in this investigation, we refer to the time slice, i.e., the number of times an action is computed for each agent in the simulation.

We model particle interactions with the two-body Weeks-Chandler-Anderson (WCA) potential [Weeks et al., 1971], which can be seen as an almost-hard-sphere interaction:

$$V = 4 \cdot V_0 \left( \left( \frac{\sigma}{r_{ij}} \right)^{12} - \left( \frac{\sigma}{r_{ij}} \right)^6 \right) + V_0. \quad (3)$$

Here,  $r_{ij} = \|\mathbf{r}_i - \mathbf{r}_j\|_2$  is the absolute distance between the particles, and  $\sigma = 2a$  the colloid diameter. We choose the interaction strength  $V_0 = k_B T$ .

## 4.2 RL Architecture

RL is a branch of machine learning in which an agent in state  $s_t$  interacts with its environment by taking action  $a_t$  that brings it to a following state  $s_{t+1}$ . The agent aims to maximize each state's scalar reward  $r_t$ . It does so by optimizing the policy  $\pi$  that governs the agent's behavior. MARL as a subfield of RL is closely related to game theory and focuses on multiple such learning agents. In addition to interacting with the environment, agents also interact with each other in cooperative or competitive ways [Littman, 1994]. At every time slice of the experiment, each agent takes an action based on its observation. Each possible action at that time is sampled with a probability determined by the policy. The Gumble-max trick [Huijben et al., 2022] is used to sample this categorical distribution efficiently. The policy is updated using a policy gradient method in which the actor takes the role of the policy and the critic evaluates the actor's performance after each episode [Sutton and Barto, 2018]. The actor and the critic are neural networks, each consisting of two dense layers with 128 neurons. The actor-critic architecture is shown in Figure 1. The Adam optimizer with a learning rate of  $\lambda = 0.001$  [Kingma and Ba, 2017] is used for the network parameter update.

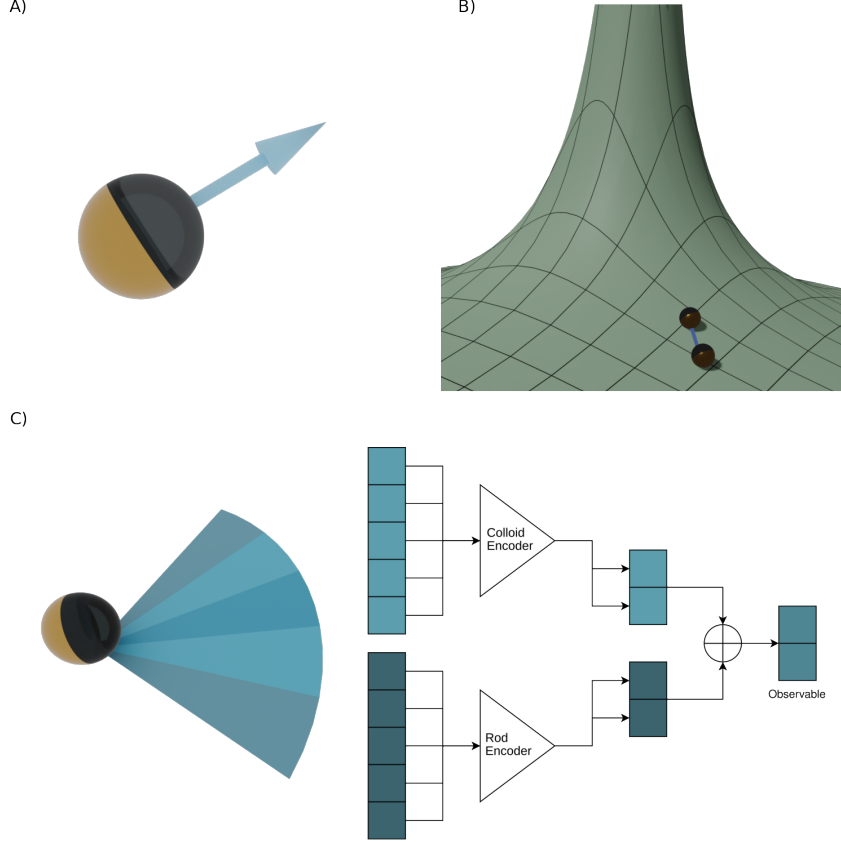


Figure 2: Various aspects of the agents deployed in this investigation. A) A representation of an ABP particle coated on one side. B) Visualization of the concentration sensing observable. C) Visualization of the vision cone observable including the trainable embedding layers.

### 4.3 Active Brownian Particles as Agents

We have used microscopic agents in all the experiments performed that mimic active Brownian particles such as the Janus particle [Walther and Müller, 2013] shown in Figure 2A). These particles can mimic active biological matter upon excitation from an outside driving force. In experimental setups, this driving force is often one or more lasers applied along a specific axis of the colloid to induce either rotation or translation. This axis is designated the *director* of the colloid and emulates a forward-facing agent. The driving mechanism is accurate enough to allow for a well-defined action space for each colloid in the system:

$$\mathcal{A} = \begin{cases} \text{Translate:} & F = 10.0, \tau = (0.0, 0.0, 0.0) \\ \text{Rotate CCW:} & F = 0.0, \tau = (0.0, 0.0, 10.0) \\ \text{Rotate CW:} & F = 0.0, \tau = (0.0, 0.0, -10.0) \\ \text{Do Nothing:} & F = 0.0, \tau = (0.0, 0.0, 0.0) \end{cases} \quad (4)$$

where  $F$  is the force magnitude in simulation units applied along the forward direction of the colloid and  $\tau$  is the torque. Another key feature of the reinforcement process is the state description parsed as an input for each agent. In this investigation, two different state descriptions, referred to hereafter as observables, are utilized.

**Concentration Sensing** The most simple observable used in the experiments is termed concentration sensing. This observable aims to replicate the sensing capabilities of biological organisms in their ability to register a change in an environmental factor such as temperature or a food source. The observable itself computes a change in the concentration of some field defined in this study as a

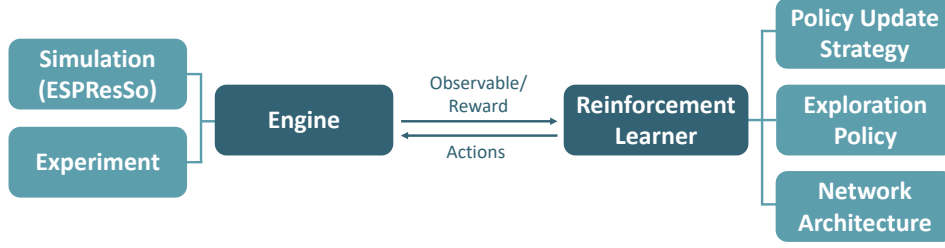


Figure 3: Simplified architecture of SwarmRL displaying data communication between the RL models and the experiments.

potential decaying like  $1/r$ . At each action update, the models receive a value computed by:

$$o_i(t) = f(\|\hat{\mathbf{r}}_i(t) - \hat{\mathbf{r}}_s(t)\|_2) - f(\|\hat{\mathbf{r}}_i(t - \Delta t) - \hat{\mathbf{r}}_s(t - \Delta t)\|_2), \quad (5)$$

where  $o_i$  is the observable for the  $i^{\text{th}}$  colloid,  $f$  is the chosen field,  $\hat{\mathbf{r}}_i(t)$  is the position of the  $i^{\text{th}}$  colloid at time  $t$ ,  $\Delta t$  is the amount of time since the last action was computed,  $\hat{\mathbf{r}}_s(t)$  is the position of the source of the potential at time  $t$ , and  $\|\cdot\|_2$  denotes a Euclidean norm. In our experiments, the source remains fixed in space and will not vary in time. The concentration sensing observable is shown graphically in Figure 2B).

**Vision Cones** The second observable employed in our studies was the vision cone shown graphically in Figure 2C). This approach mimics an agent with the ability to identify particle species and a blurred sense of direction, that is, a range of angles within which it knows other particles are present. In this study, the vision cone is broken into five components. Each component of the vision cones computes  $N$  numbers where  $N$  is the number of unique species in the system, e.g., for rod rotation, there are active particles and rod particles resulting in  $N = 2$ . The value of the cone is computed by:

$$o_i^{jk} = \sum_{n \in \mathcal{C}_j} \frac{1}{\|\mathbf{r}_i - \mathbf{r}_n^k\|_2}, \quad (6)$$

where  $o_i^{jk}$  is the observable of the  $i^{\text{th}}$  particle for the  $j^{\text{th}}$  vision cone computed for all particles of species  $k$  which lie within the cone represented by  $\mathcal{C}_j$ . In order to provide this information to an actor and critic, we implemented an embedding scheme. In this scheme, the vision cone values associated with the rods and colloids are split into two vectors and passed through their trainable embedding layers, producing a reduced, 2-dimensional output. Element-wise addition of these vectors forms the final observable used to compute actions. The embedding layers are trained along with the actor and critic during the simulations, allowing each model to learn a representation of its environment.

#### 4.4 SwarmRL

The RL performed in this investigation is part of a project involved with not only training microswimmers but also deploying trained models in natural experiments. Therefore, all of the infrastructure surrounding the training of the agents and deployment in the ESPResSo simulation engine has been written into an open-source Python package SwarmRL. As illustrated in Figure 3, SwarmRL provides an interface to each component of the RL pipeline as well as different *environments* including both the simulation engine and actual experiment setups. SwarmRL is built on the JAX [Bradbury et al., 2018] ecosystem and utilizes Flax [Heek et al., 2023] for neural networks. SwarmRL is publicly available on GitHub at <https://github.com/SwarmRL/SwarmRL>.

## 5 Experiments

This investigation performs two experiments: source detection and rod rotation. Each task requires a differing degree of complexity, and in each case, the agents discover different strategies depending on their environment. Training for each task occurs in the same way. Each model is trained with ten agents for a total of 10,000 episodes. The first 5000 episodes are performed using an exploration rate of 20%; that is, 20% of the time, colloids chose a random action other than that provided by the

actor. The second 5000 episodes were performed without this exploration policy. This is performed for ten ensembles with different starting simulation conditions and neural network initialization. In all computations, an average value over these ensembles is computed, resulting in the corresponding error values. At the end of the training, all the trained models are used in production simulations of 5.000.000 time-steps. This procedure was carried out for five different temperatures: {0 K, 150 K, 273 K, 300 K, 350 K } to explore the changes in emergent strategy and efficacy of chosen strategy.

### 5.1 Source Detection

The simplest task tested was that of source detection. In this case, the colloids have a biologically inspired sense of smell; they can sense changes in some applied concentration field. Their reward is based on changes in this field, i.e., moving closer to the source of the concentration yields a better reward. Such a task is reminiscent of chemo-taxis in bacteria [Zhuang and Sitti, 2016] or, theoretically, detection of a drug delivery site in medicinal micro-robotics [Schmidt et al., 2020]. Mathematically, the reward closely resembles the observables of these colloids:

$$r_i = \alpha \cdot \text{Clip} \left( \frac{1}{\|\hat{\mathbf{r}}_i(t) - \hat{\mathbf{r}}_s(t)\|_2} - \frac{1}{\|\hat{\mathbf{r}}_i(t-1) - \hat{\mathbf{r}}_s(t-1)\|_2}, 0, \text{None} \right) \quad (7)$$

where  $\alpha$  is some reward scaling value, the clip operation ensures that particles are rewarded for moving toward the source and receive no input if they move away. The experiment results are outlined in Figure 4. Figure 4A) illustrates the policy breakdown for inputs to the neural network at different temperatures. To construct these plots, we pass artificial data through the trained models and compute the probability of different actions for these inputs. We see that negative inputs in each temperature, i.e., a movement towards lower values of the concentration field, result in increased rotation probability and decreased translation. This is opposed to movements towards the source, which increases translation probability. Such a learned policy is reminiscent of run-and-tumble motion in bacteria in response to changing environments [van Ginkel et al., 2021]. It appears that at all temperatures, the *Do Nothing* actions is never included in the learned strategy and remains a randomly selected action. We also noticed in these experiments that once the agents learned to rotate either clockwise or counterclockwise, they did not use the other action.

Figure 4B), C), and D) illustrate the distance of the colloids from the source at different temperatures. In Figure 4C), the colloids trained at higher temperatures converge faster onto the source. This is expanded upon in 4D) where the histograms of the equilibrium region are plotted for each temperature. These histograms show that models trained at higher temperatures converge closer to the source of the field and, in general, experience less variance around it. This is generally true; however, it can also be seen that the 150 K model reached the closest to the source while higher temperatures moved back away. The mechanism behind this improved policy can be understood by looking directly at the trajectories of the models in Figures 4E) and F). In the 0K simulation shown in 4E), the colloids undertake an orbital movement towards the source and, in doing so, maximize their reward over time. In the case of a 350 K environment shown in 4F), the colloids cannot afford to take such a policy as the random fluctuations will push them out of their orbit. In these cases, the colloids move more directly toward the source and perform more oscillatory movement once they are close. This approach explains the improved proximity of the higher temperature models as they orient themselves to move directly to their target. However, the stronger the Brownian forces acting on the colloids, the harder it will be to remain close to the source and the more significant are their fluctuations around it. In summary, including Brownian forces in the model training results in a more direct approach to the source of the field attracting the colloids. This policy results in closer average distances to the source and less variation around the it.

### 5.2 Rod Rotation

Increasing the complexity of our experiments, the subsequent investigation involved training the agents to rotate a rod. In these experiments, the rod is modeled as a series of rigidly bonded small colloids so that they cannot move away from one another. This task is interesting as the colloids should cooperate to achieve this task efficiently. The observables we use in the rod rotation experiments are the vision cones discussed in Section 4.3, which return values for both the agents and the rod colloids. The rewards for this task are broken into two components, detecting the rod and increasing its angular

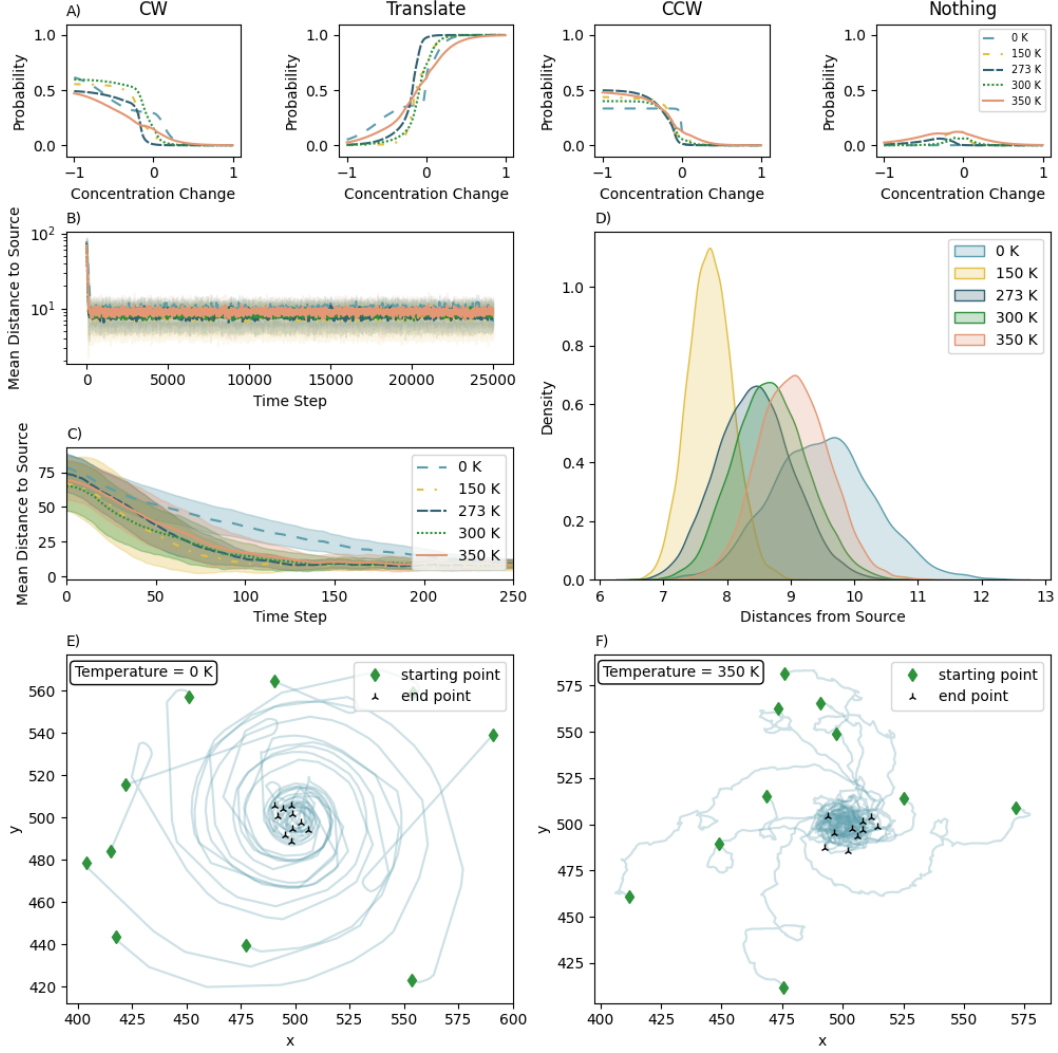


Figure 4: A) The policy evaluation performed on trained actors. Each figure shows the probability of taking a certain action given the input to the network. B) The mean distance of all agents to the source in the simulation as a function of time. Different line styles and colors correspond to different temperatures. C) A zoomed-in frame of B) where the higher temperature models converge faster and closer to the source of their sensing field. D) Histograms computed on the converged regions of the trajectory. E)-F) Example trajectory of the agents at 0 K and 350 K respectively.

velocity. Rod detection is encouraged by rewarding the agents if they move closer to the rod particles:

$$r_i^{\text{rod proximity}} = \sum_j \frac{1}{|\hat{\mathbf{r}}_i(t) - \hat{\mathbf{r}}_j(t)|} - \sum_j \frac{1}{|\hat{\mathbf{r}}_i(t - \Delta t) - \hat{\mathbf{r}}_j(t - 1)|}, \quad (8)$$

where  $\hat{\mathbf{r}}_j$  are all particles in the rod. The reward for the rod rotation itself is more involved as a partitioning scheme is used in order to compute a meaningful single-agent contribution which is applied to the total reward as:

$$r_i^{\text{rod rotation}} = \frac{\tau_i}{\tau_{\text{net}}} \cdot (\omega_{\text{rod}}(t) - \omega_{\text{rod}}(t - \Delta t)), \quad (9)$$

where  $\tau_i$  is the torque exerted on the rod by colloid  $i$ ,  $\tau_{\text{net}}$  is the net torque acting on the rod, and  $\omega_{\text{rod}}(t)$  is the angular velocity of the rod at time  $t$ . The final reward for the colloid is then computed with the following:

$$r_i = \alpha \cdot r_i^{\text{rod proximity}} + \beta \cdot r_i^{\text{rod rotation}}, \quad (10)$$



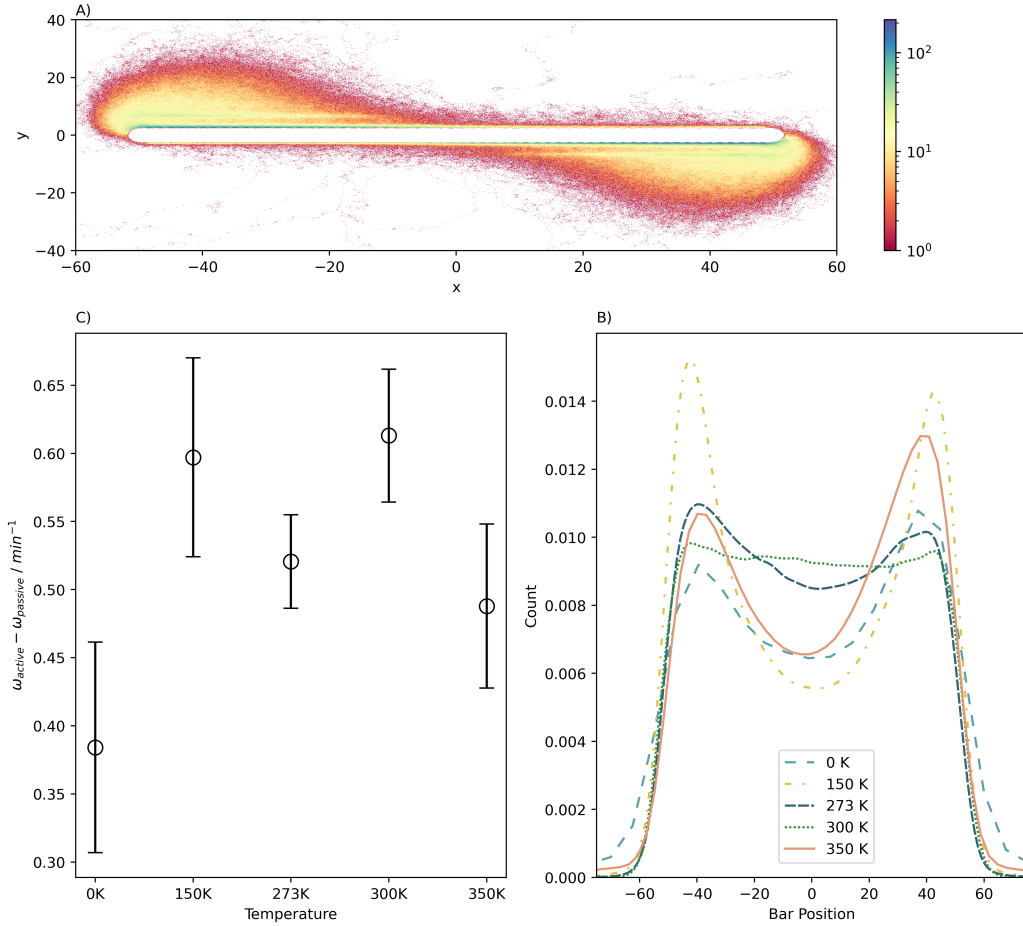


Figure 5: A) The 2D histogram formed using the trajectory of a single 150 K deployment simulation. B) The rod’s angular velocity minus the corresponding value for a system without agents as a function of temperature. C) A histogram along the rod’s long axis demonstrates the accumulation at the ends of the rod for each temperature.

where  $\alpha$  and  $\beta$  are scaling factors chosen in this work to be 10 and 100, respectively, such that successful rod rotation dominates the reward. The results of the rod rotation experiment are outlined in Figures 5 A)-C). During the rod rotation experiments, two observables were of interest: the angular velocity of the rod, which measures the agents’ efficacy, and the agents’ distribution along the rod, which provides a description of their strategy. Figure 5B) shows the average absolute rod velocity as a function of temperature. In order to account for the natural motion of the rod, simulations have been performed without active colloids and these rod velocities subtracted from the active values. It is clear from the measurements that the agents are capable of achieving greater rod velocities at higher temperatures. This is of interest as the 0 K simulation provides the least resistance to rotation as no effects of the Brownian motion present. As the temperature continues to increase, the mean rod velocity oscillates and decreases, suggesting that at some stage, the random fluctuations again become problematic for the agents’ strategy.

The policy of the agents can be seen in Figures 5 A) and C). Figure 5A) plots the 2D histogram of the colloids for one of the 150 K simulation. It is evident in this plot that the agents form on either end of the rod in a manner that maximises the applied torque. A clearer picture of this strategy emerges when studying only the single-dimensional histogram along the long axis of the rod, shown in Figure 5C). Here we can see that concentration along the ends of the rod is an emergent strategy for all temperatures. This concentration is maximized at 150 K, possibly explaining the enhanced angular velocity in Figure 5C). As temperature increases it seems that the agents move towards the

center of the rod, perhaps preventing them from sliding off due to the additional random forces. This trend is broken in the 350 K simulation where the agents once again form on the ends of the rod, although in a more asymmetric fashion, perhaps suggesting an alternative strategy in these conditions.

## 6 Conclusion and Outlook

We have performed experiments using the ESPResSo simulation engine to understand how temperature impacts the emergent strategy and efficacy of these strategies in micro-scale agents governed by MARL. In the location detection experiments resembling biological chemotaxis, we found that increasing the temperature resulted in the agents taking direct approaches toward the source of the field. In contrast, with no Brownian motion, they entered a decaying orbit. This was accompanied by the agents equilibrating closer to the source at higher temperatures, suggesting the strategy was more effective than orbiting. The most exciting outcome was the policy adopted by the agents as we saw them take the translation action upon a move closer to the source and more rotation as they moved away. This approach strategy is heavily reminiscent of bacterial run and tumble motion. Rod rotation also demonstrated an evolving strategy with temperature as we saw the colloids favor sitting on the ends of the rods, thereby maximizing the applied torque. However, after 150 K the colloids began to favor moving inwards along the rod, presumably to avoid sliding off during rotation. These results demonstrate that the environments of microscopic, intelligent agents profoundly impact their efficacy and the strategies they need to adopt to achieve different tasks. Continued work in this area could look into more efficient training strategies to achieve the performance of the models at 150 K in the 350 K simulations. Further, training models in simulation environments to be robust against these environmental factors could result in a smaller generalization gap for crossing into physical experiments. Micro-robotics and MARL are, without a doubt, technologies of the future. The key to unlocking their success lies in understanding the conditions under which they will work and using these to their advantage.

## 7 Acknowledgements

V.L.H and C.B acknowledge funding from the DFG Centre of Excellence 2117, Germany "Centre for the Advances Study of Collective Behaviour", ID: 422037984. C.H and S.T acknowledge financial support from the German Funding Agency (Deutsche Forschungsgemeinschaft DFG) under Germany's Excellence Strategy EXC 2075-390740016, and S. T was supported by a LGF stipend of the state of Baden-Württemberg. C.H, and S.T acknowledge financial support from the German Funding Agency (Deutsche Forschungsgemeinschaft DFG) under the Priority Program SPP 2363.

## References

- Tobias Bäuerle, Robert C. Löffler, and Clemens Bechinger. Formation of stable and responsive collective states in suspensions of active colloids. *Nature Communications*, 11(1):2547, May 2020. ISSN 2041-1723. doi: 10.1038/s41467-020-16161-4. URL <https://doi.org/10.1038/s41467-020-16161-4>.
- Francesco Borra, Luca Biferale, Massimo Cencini, and Antonio Celani. Reinforcement learning for pursuit and evasion of microswimmers at low Reynolds number. *Phys. Rev. Fluids*, 7:023103, Feb 2022. doi: 10.1103/PhysRevFluids.7.023103. URL <https://link.aps.org/doi/10.1103/PhysRevFluids.7.023103>.
- James Bradbury, Roy Frostig, Peter Hawkins, Matthew James Johnson, Chris Leary, Dougal Maclaurin, George Necula, Adam Paszke, Jake VanderPlas, Skye Wanderman-Milne, and Qiao Zhang. JAX: composable transformations of Python+NumPy programs, 2018. URL <http://github.com/google/jax>.
- Peter G. Brewer, Edward T. Peltzer, and Kathryn Lage. Life at low Reynolds number re-visited: The efficiency of microbial propulsion. *Deep Sea Research Part I: Oceanographic Research Papers*, 185:103790, 2022. ISSN 0967-0637. doi: <https://doi.org/10.1016/j.dsr.2022.103790>. URL <https://www.sciencedirect.com/science/article/pii/S0967063722001030>.

- Chun-Jen Chen and Clemens Bechinger. Collective response of microrobotic swarms to external threats. *New Journal of Physics*, 24(3):033001, mar 2022. doi: 10.1088/1367-2630/ac5374. URL <https://dx.doi.org/10.1088/1367-2630/ac5374>.
- Benedikt Hartl, Maximilian Hübl, Gerhard Kahl, and Andreas Zöttl. Microswimmers learning chemotaxis with genetic algorithms. *Proceedings of the National Academy of Sciences*, 118(19):e2019683118, 2021. doi: 10.1073/pnas.2019683118. URL <https://www.pnas.org/doi/abs/10.1073/pnas.2019683118>.
- Jonathan Heek, Anselm Levskaya, Avital Oliver, Marvin Ritter, Bertrand Rondepierre, Andreas Steiner, and Marc van Zee. Flax: A neural network library and ecosystem for JAX, 2023. URL <http://github.com/google/flax>.
- Iris A. M. Huijben, Wouter Kool, Max B. Paulus, and Ruud J. G. van Sloun. A review of the gumbel-max trick and its extensions for discrete stochasticity in machine learning, 2022.
- Diederik P. Kingma and Jimmy Ba. Adam: A method for stochastic optimization, 2017.
- Sven Krippendorf and Michael Spannowsky. A duality connecting neural network and cosmological dynamics. *Machine Learning: Science and Technology*, 3(3):035011, aug 2022. doi: 10.1088/2632-2153/ac87e9. URL <https://dx.doi.org/10.1088/2632-2153/ac87e9>.
- François A. Lavergne, Hugo Wendehenne, Tobias Bäuerle, and Clemens Bechinger. Group formation and cohesion of active particles with visual perception-dependent motility. *Science*, 364(6435):70–74, 2019. doi: 10.1126/science.aau5347. URL <https://www.science.org/doi/abs/10.1126/science.aau5347>.
- Michael L. Littman. Markov games as a framework for multi-agent reinforcement learning. In William W. Cohen and Haym Hirsh, editors, *Machine Learning Proceedings 1994*, pages 157–163. Morgan Kaufmann, San Francisco (CA), 1994. ISBN 978-1-55860-335-6. doi: <https://doi.org/10.1016/B978-1-55860-335-6.50027-1>. URL <https://www.sciencedirect.com/science/article/pii/B9781558603356500271>.
- Alberto Lolli, Giovanni Corsi, and Antonio DeSimone. Control and navigation problems for model bio-inspired microswimmers. *Meccanica*, 57(10):2431–2445, Oct 2022. ISSN 1572-9648. doi: 10.1007/s11012-022-01567-9. URL <https://doi.org/10.1007/s11012-022-01567-9>.
- Clément Moreau, Kenta Ishimoto, Eamonn A. Gaffney, and Benjamin J. Walker. Control and controllability of microswimmers by a shearing flow. *Royal Society Open Science*, 8(8):211141, 2021. doi: 10.1098/rsos.211141. URL <https://royalsocietypublishing.org/doi/abs/10.1098/rsos.211141>.
- S. Muiños-Landin, A. Fischer, V. Holubec, and F. Cichos. Reinforcement learning with artificial microswimmers. *Science Robotics*, 6(52):eabd9285, 2021. doi: 10.1126/scirobotics.abd9285. URL <https://www.science.org/doi/abs/10.1126/scirobotics.abd9285>.
- Ke Qin, Zonghao Zou, Lailai Zhu, and On Shun Pak. Reinforcement learning of a multi-link swimmer at low Reynolds numbers. *Physics of Fluids*, 35(3), 03 2023. ISSN 1070-6631. doi: 10.1063/5.0140662. URL <https://doi.org/10.1063/5.0140662>. 032003.
- Christine K. Schmidt, Mariana Medina-Sánchez, Richard J. Edmondson, and Oliver G. Schmidt. Engineering microrobots for targeted cancer therapies from a medical perspective. *Nature Communications*, 11(1):5618, Nov 2020. ISSN 2041-1723. doi: 10.1038/s41467-020-19322-7. URL <https://doi.org/10.1038/s41467-020-19322-7>.
- Fernando Soto, Jie Wang, Rajib Ahmed, and Utkan Demirci. Medical Micro/Nanorobots in precision medicine. *Adv Sci (Weinh)*, 7(21):2002203, October 2020.
- Takuma Sugi, Hiroshi Ito, and Ken H Nagai. Collective pattern formations of animals in active matter physics. *Biophys Physicobiol*, 18:254–262, October 2021.
- Richard S. Sutton and Andrew G. Barto. *Reinforcement Learning: An Introduction*. The MIT Press, second edition, 2018. URL <http://incompleteideas.net/book/the-book-2nd.html>.

- Bart van Ginkel, Bart van Gisbergen, and Frank Redig. Run-and-tumble motion: The role of reversibility. *Journal of Statistical Physics*, 183(3):44, Jun 2021. ISSN 1572-9613. doi: 10.1007/s10955-021-02787-1. URL <https://doi.org/10.1007/s10955-021-02787-1>.
- Andreas Walther and Axel H. E. Müller. Janus particles: Synthesis, self-assembly, physical properties, and applications. *Chemical Reviews*, 113(7):5194–5261, 2013. doi: 10.1021/cr300089t. URL <https://doi.org/10.1021/cr300089t>. PMID: 23557169.
- John D Weeks, David Chandler, and Hans C Andersen. Role of repulsive forces in determining the equilibrium structure of simple liquids. *The Journal of chemical physics*, 54(12):5237–5247, 1971.
- Florian Weik, Rudolf Weeber, Kai Szuttor, Konrad Breitsprecher, Joost de Graaf, Michael Kuron, Jonas Landsgesell, Henri Menke, David Sean, and Christian Holm. Espresso 4.0 – an extensible software package for simulating soft matter systems. *The European Physical Journal Special Topics*, 227(14):1789–1816, Mar 2019. ISSN 1951-6401. doi: 10.1140/epjst/e2019-800186-9. URL <https://doi.org/10.1140/epjst/e2019-800186-9>.
- Viktor Zaverkin, David Holzmüller, Luca Bonferraro, and Johannes Kästner. Transfer learning for chemically accurate interatomic neural network potentials. *Phys. Chem. Chem. Phys.*, 25:5383–5396, 2023. doi: 10.1039/D2CP05793J. URL <http://dx.doi.org/10.1039/D2CP05793J>.
- Jiang Zhuang and Metin Sitti. Chemotaxis of bio-hybrid multiple bacteria-driven microswimmers. *Scientific Reports*, 6(1):32135, Aug 2016. ISSN 2045-2322. doi: 10.1038/srep32135. URL <https://doi.org/10.1038/srep32135>.
- Andreas Zöttl and Holger Stark. Modeling active colloids: From active brownian particles to hydrodynamic and chemical fields. *Annual Review of Condensed Matter Physics*, 14(1):109–127, 2023. doi: 10.1146/annurev-conmatphys-040821-115500. URL <https://doi.org/10.1146/annurev-conmatphys-040821-115500>.
- Andreas Zöttl and Holger Stark. Emergent behavior in active colloids. *Journal of Physics: Condensed Matter*, 28(25):253001, may 2016. doi: 10.1088/0953-8984/28/25/253001. URL <https://dx.doi.org/10.1088/0953-8984/28/25/253001>.